

Title:

Predicting movement intentions from local field potentials in humans: What neuronal decoding tells us about motor encoding.



Authors:

Etienne Combrisson^{1,2,3}, Franck Di Rienzo², Marcela Perrone-Bertolotti⁴, Juan LP Soto⁵, Philippe Kahane⁴, J-P Lachaux³, Aymeric Guillot², Karim Jerbi¹

Affiliations:

¹ Psychology Department, University of Montreal, QC, Canada

² Univ Lyon, Université Claude Bernard Lyon 1, Laboratoire Interuniversitaire de Biologie de la Motricité, EA 7424, F69622 Villeurbanne, Cedex, France



³ Lyon Neuroscience Research Center, Brain Dynamics and Cognition, INSERM U1028, UMR 5292, Lyon University

⁴ Neurology Dept and GIN U836 INSERM-UJF-CEA, Grenoble University Hospital, Grenoble, France

⁵ Telecommunications and Control Engineering Department, University of Sao Paulo, Sao Paulo, Brazil

Corresponding author

Etienne Combrisson

Address:

Psychology Department
University of Montreal
Pavillon Marie-Victorin
90, avenue Vincent d'Indy, Quebec, Canada
E-mail address: e.combrisson@gmail.com

Outline

1. Abstract.....	3
2. Significance Statement.....	3
3. Introduction.....	4
4. Material and methods.....	6
4.1. Participants.....	6
4.2. Electrode implantation and Stereotactic EEG recordings.....	6
4.3. Experimental design.....	7
4.4. Data preprocessing.....	7
4.5. Spectral analyses.....	8
4.5.1. Filtering and complex decomposition.....	8
4.5.2. Power features estimation.....	8
4.5.3. Instantaneous phase features estimation.....	9
4.5.4. Phase-Amplitude Coupling (PAC) features estimation.....	9
4.6. Signal Classification.....	11
4.6.1. Single feature evaluation.....	11
4.6.2. Intra-site multi-features.....	12
4.6.3. Statistical evaluation and visualization of decoding performances.....	12
4.6.4. Multi-features selection.....	12
5. Results.....	14
5.1. Decoding motor intentions and execution using power and phase features.....	14
5.2. Time resolved power modulations and decoding.....	15
5.3. Temporal Generalization of movement direction decoding.....	16
5.4. Feature combination on deep sources.....	16
5.5. Example of a time resolved multi-feature selection.....	17
5.6. Decoding results of the multi-feature procedure across subjects.....	20
6. Discussion.....	21
6.1. Unraveling the role of power, phase and phase-amplitude coupling.....	21
6.2. Involvement of non-primary motor areas.....	21
6.3. Features specificity and complementarity.....	22
6.4. Limitations and future paths.....	22
Acknowledgments.....	23
Conflict of interest.....	23
7. References.....	24

1. Abstract

(temporary version / will be updated with some additional data)

Intracranial EEG (iEEG) recordings from the human motor cortex can be used to infer motor parameters such as limb movement direction or kinematics. Most studies so far have demonstrated the feasibility of movement decoding using spectral power recorded in sensorimotor areas. However, whether other spectral features such as oscillatory phase and cross-frequency measures provide additional information to decode movement plans is still unclear. Here, we investigate the feasibility of using three features of neuronal oscillations, phase, amplitude and Phase-Amplitude Coupling (PAC) to classify movement directions using multi-site invasive recordings obtained during execution but also during movement planning. To this end, we recorded intracranial EEG data from 6 patients while they performed a delayed center-out motor task (up, down, right or left). The instantaneous phase, amplitude and PAC were computed in multiple frequency bands using the Hilbert transform and the obtained features were used to train a classifier to decode movement directions (a) during the execution, and (b) during the pre-movement delay-period. Movement directions were decoded using linear discriminant analysis. Our findings demonstrate that the best decoding performances were obtained using power, but that phase and PAC also provide statistically significant movement decoding. The combination of the features in a multi-feature decoding framework allowed for increased decoding accuracy not only during execution, but also during the preceding action planning phase. Interestingly, we also found significant temporal generalizations of the decoding: Training a movement classifier on the execution data allowed for significant decoding of movement intentions in the delay period before movement onset. These findings may have implications for research on brain-computer interfaces and they extend our understanding of the role of brain-wide neuronal oscillations in motor encoding.

Keywords:

Movement decoding, Intentions, Brain decoding, intracranial EEG, amplitude, phase, phase-amplitude coupling

2. Significance Statement

3. Introduction

Moto-neurons might seem to be obstinate, but they have a preferred direction. This phenomenon known as directional tuning (DT) means that their activity increase at a specific direction angle (Georgopoulos et al., 1982, 1986) and the complex synchronization / desynchronization of assembly of neurons finally produced the smoothed movement. This behavior is largely referenced at the spiking scale (SUA and MUA) for animal (Taylor, 2002; Heldman et al., 2006) and human recordings (Linkens et al., 2009). SUA provide the highest spatial and temporal resolution at the cost of being the most invasive recording type, difficult to maintain for long term support and with the complexity of spike sorting algorithms. In this context, it has been demonstrated that LFP signals shared directional informations with SUA and MUA and can also be used to decode movement parameters (Mehring et al., 2003; Rickert, 2005; Liu and Newsome, 2006; Schalk et al., 2007; Chao, 2010). Since then, the Brain-Computer Interface (BCI) community explore it as a potential motor control (Leuthardt et al., 2004; Ball et al., 2009). The LFP signal is generally obtained by taking low-passed spiking activity (ca. 250 hz), subdural grids and strips of electrodes or using stereotactically implanting multiple multi-lead depth electrodes (stereo-EEG or SEEG) (Kahane et al., 2003). This latest and rare intracranial recordings are generally obtained in the context of presurgical evaluation in patients with drug-resistant epilepsy and allow spectral investigations for frequencies up to 250 hz.

Décodage de l'intention :

- (Gallivan et al., 2011) show significant grasping vs touching task decoding in human fronto-parietal network using fMRI

These clinical recordings are either performed via subdural grids and strips of electrodes or by stereotactically implanting multiple multi-lead depth electrodes, a procedure known as stereo-EEG (SEEG) . Because of the type of electrodes, the sampling frequency and amplifiers routinely used in this clinical setting, the recorded signals do not capture the SUA and MUA of the neuronal populations but rather the LFP signal (ca. <250 Hz). Both techniques allow for the investigation of task-related changes in signal power in various frequency bands ranging from delta (2-4 Hz), theta (4-7 Hz), alpha (8-12 Hz), beta (15-30 Hz) to gamma (up to ~250 Hz) frequencies (REFs). A large body of intracranial EEG (iEEG) research has shown that movement execution leads to significant power modulations in multiple frequency components of the LFP signal in motor cortex (REFs). More recently, a number of invasive studies with epilepsy patients report that iEEG recordings from the human motor cortex show directional tuning (REFs). Interestingly, when comparing the decoding power achieved by the different frequency components of the ECoG signal, the latter studies show that the highest directional tuning (and hence decoding power) was found in the low-pass filtered signals (e.g. <4 Hz) and in the amplitude modulation of the so-called high gamma band (approx. 60-140 Hz). This observation is in agreement with data on directional tuning reported previously in monkeys (REFs) and non-invasively in humans (REFs).

While the above studies provide strong evidence for the possibility to decode limb movements using spectral power predominantly from motor cortex, it is still not clear whether other frequency-domain features such as oscillatory phase and cross-frequency measures provide additional information to decode movement parameters. Here, we investigate the feasibility of using three

features of neuronal oscillations, which are phase, amplitude and Phase-Amplitude Coupling (PAC) to classify movement directions using multi-site invasive recordings obtained during execution but also during movement planning. Importantly, we were able to explore this question via a rare access to direct intracerebral recordings in human subjects (over 600 multi-site LFP recordings).

Our findings indicate that the best movement decoding performances were obtained using power, but that phase and PAC also provide statistically significant movement direction decoding. The combination of the features in a multi-feature decoding framework allowed for increased decoding accuracy not only during execution, but even during action planning. We also observed temporal generalizations of the decoding across the various phases of the delayed motor task.

Direction decoding : (Waldert et al., 2008; Wang et al., 2012)
Intentions decoding : (Gallivan et al., 2011; Lew et al., 2014)

(Waldert et al., 2007)

4. Material and methods

4.1. Participants

Six patients with medically intractable epilepsy participated in this study (6 females, mean age 22.17 ± 4.6). The patients were stereotactically implanted with multi-lead EEG depth electrodes at the Epilepsy Department of the Grenoble Neurological Hospital (Grenoble, France). In collaboration with the medical staff, and based on visual inspection, electrodes presenting pathological waveforms were discarded from the present study. All participants provided written informed consent, and the experimental procedures were approved by the Institutional Review Board, as well as by the National French Science Ethical Committee. Patient-specific clinical details can be found in Table 1.

	Handedness	Age	Gender	Epilepsy type	Etiology	EZ localization	Lesion
P1	R	19	F	Frontal	Secondary	Precentral gyrus (RH)	Dysplasia
P2	R	23	F	Frontal	Cryptogenic	Precentral gyrus (LH)	Absent
P3	R	18	F	Frontal	Cryptogenic	Fronto-basal (RH)	Absent
P4	R	18	F	Frontal	Idiopathic	Fronto-central (RH)	Absent
P5	R	31	F	Insula	Secondary	Operculum (RH)	Cavernoma
P6	R	24	F	Frontal	Secondary	Supra-sylvian posterior (LH)	Vascular sequelae

Table 1. Patient data: age, gender, and broad description of epilepsy type as determined by the clinical staff of the Grenoble Neurological Hospital, Grenoble, France (Recording sites with epileptogenic activity were excluded from the analyses).

4.2. Electrode implantation and Stereotactic EEG recordings

Each patient was implanted with stereotactic electroencephalography (SEEG) electrodes. Each one of these had a diameter of 0.8 mm and, depending on the implanted structure, was composed of 10 to 15 contacts that were 2 mm wide and 1.5 mm apart (DIXI Medical Instrument). Intracranial EEG signals were recorded from a total of 748 intracerebral sites across all patients (126 sites in each participant, except for one patient who had 118 recording sites). At the time of acquisition, a white matter electrode was used as reference, and data was bandpass filtered from 0.1 to 200 Hz and sampled at 1024 Hz. Electrode locations were determined using the stereotactic implantation scheme and the Talairach and Tournoux proportional atlas (Talairach and Tournoux, 1993). The electrodes were localized in each individual subject in Talairach coordinates (based on post-implantation CT), and then transformed to standard MNI coordinate system according to standard routines and previously reported procedures (Jerbi et al., 2009, 2010; Ossandon et al., 2011; Bastin et al., 2016).

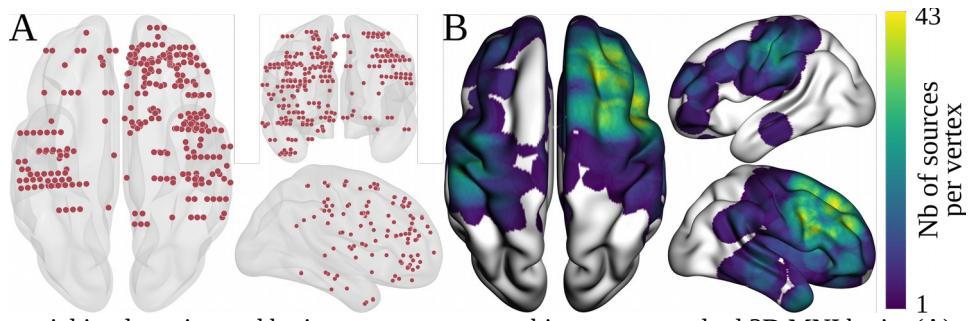


Figure 1. Intracranial implantation and brain coverage across subjects on a standard 3D MNI brain. (A) top, front and right view of deep recording sites, (B) top, left and right view of the number of contributing sources per vertex.

4.3. Experimental design

The experimental design used in this study is a delayed center-out motor task. After a rest period of 1000ms, the participants were visually cued to prepare a movement towards a visually presented target in one of four possible directions: up, down, left or right (*Planning phase*). Next, after a 1500 ms delay period, a Go signal prompted the subjects to move the cursor towards the target (*Execution Phase*). The Go signal consisted of a central cue changing from white to black. Figure 1c shows the task design.

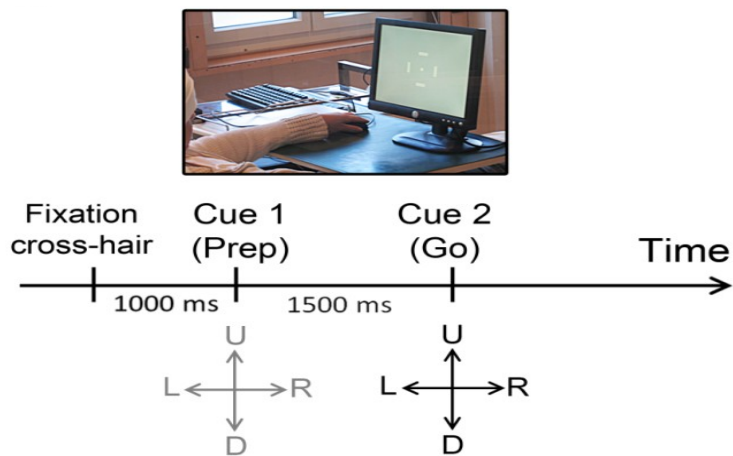


Figure 2. Relative power modulations per directions (up/right/down/left) for a premotor seeg site. (A) Time-frequency representation (B) Single-trial high gamma [60, 200Hz] power modulation.

4.4. Data preprocessing

SEEG data preprocessing was conducted according to our routine procedures (Jerbi et al., 2009; Bastin et al., 2016). These included signal bipolarization, where each electrode site was re-referenced to its direct neighbor. Bipolar re-referencing can increase sensitivity and reduce artefacts by canceling out distant signals that are picked up by adjacent electrode contacts (e.g. mains power). The spatial resolution of bipolar SEEG of our electrodes were approximately 3mm (Lachaux et al., 2003; Kahane et al., 2006; Jerbi et al., 2009). Next, using visual inspection and time-frequency explorations of the signal, we excluded electrodes containing pathological epileptic activity. In addition, electrodes located close to the extra-ocular eye muscles were systematically

excluded to avoid eye-movement contaminations in our analyses. The pre-processing led to a total of 580 bipolar derivations across all participants

4.5. Spectral analyses

In order to explore amplitude and phase relationship and their decoding utilities, we explored a variety of spectral features including power, phase and phase-amplitude coupling. We investigated several frequency bands including very low frequency component (VLFC) [0.1; 1.5Hz], delta (δ) [2-4Hz], theta (θ) [5-7Hz], alpha (α) [8-13Hz], beta (β) [13-30Hz], low-gamma (low γ) [30-60Hz] and broadband gamma (high γ) [60-200Hz]. Power features were computed in the 6 following bands δ , θ , α , β , low- γ and high- γ . Phase were extracted from 4 bands (VLFC, δ , θ and α). Phase amplitude coupling was finally conducted by taking δ , θ and α phase coupled with high- γ . Furthermore, in order to see time decoding evolutions, we systematically conserve time dimension by considering several points across time. The choice of windows is specific to each attribute and will be describe in their respective sub-sections below but, at the end, each feature will have 67 time points. For each seeg site, there is 13 features (6 of power, 4 of phase and 3 of pac) with 67 time points. Across all eeg site, this lead to a total of 505180 independent features to classify.

4.5.1. Filtering and complex decomposition

To have a methodological consistency, band-specific features were filtered using a two-way zero-phase lag least squares FIR filter, equivalent to the *eegfilt.m* function implemented in the EEGLAB toolbox (Delorme and Makeig, 2004). Then, on filtered signals, phase and amplitude are respectively deduced from the angle and the module of the complex signal given by the Hilbert transform.

4.5.2. Power features estimation

Power extraction: From the band-specific Hilbert transform, power modulations were computed by taking the square of time resolved amplitude. For the specific case of high-gamma band, the [60, 200Hz] was splitted into 10Hz non-overlapping sub-bands and final gamma power modulations are obtained by taking the mean of those multiple sub-bands, according to our previous routines (Jerbi et al., 2009; Ossandon et al., 2011; Perrone-Bertolotti et al., 2012; Vidal et al., 2012, 2014; Hamamé et al., 2014; Bastin et al., 2016).

Time resolution: power was averaged using a 700ms sliding window, with a 50ms shifting, leading to 67 time points. The classification is applied on unnormalized power. We applied a normalization only for the specific case of the visualization (time-frequency maps and single trial representation, see **Fig 3**). To this end, to each frequency band, we subtract then divide by the mean of a 500ms baseline window, centered during the pre-stimulus rest period ([-750ms, -250ms]).

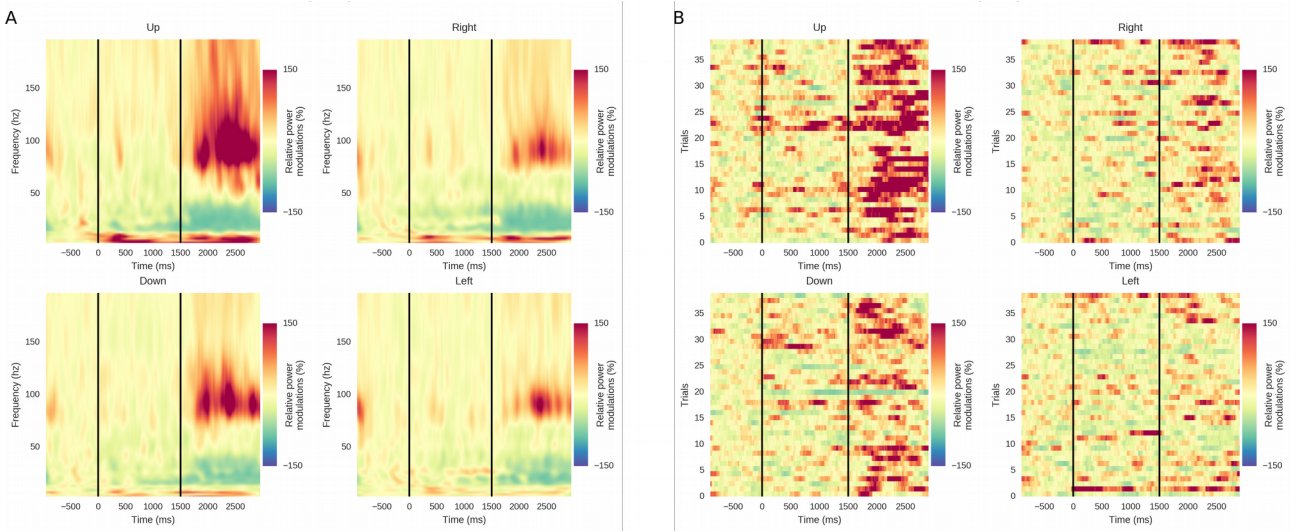


Figure 3. Relative power modulations per directions (up/right/down/left) for a premotor seeg site. (A) Time-frequency representation (B) Single-trial high gamma [60, 200Hz] power modulation.

4.5.3. Instantaneous phase features estimation

Phase extraction: For a specific frequency band, phase features are extracted from the angle of the Hilbert transform. For the case of classification, from this instantaneous phase, we selected of point every 50ms. Finally, we used the Rayleigh's test to estimate significant phase modulations (Tallon-Baudry et al., 1996; Babiloni et al., 2002; Lakatos, 2005), using the circular statistics toolbox (Berens and others, 2009). This instantaneous phase is then used for the classification. To observe phase-alignment consistency across trials, we compute the Phase Locking Factor (PLF) which is defined as the mean across modulus of single trial phase (Tallon-Baudry et al., 1996).

Time resolution: to have a consistency with power features, we selected instantaneous phase at each center of above defined power windows, which led to 67 phase points across time.

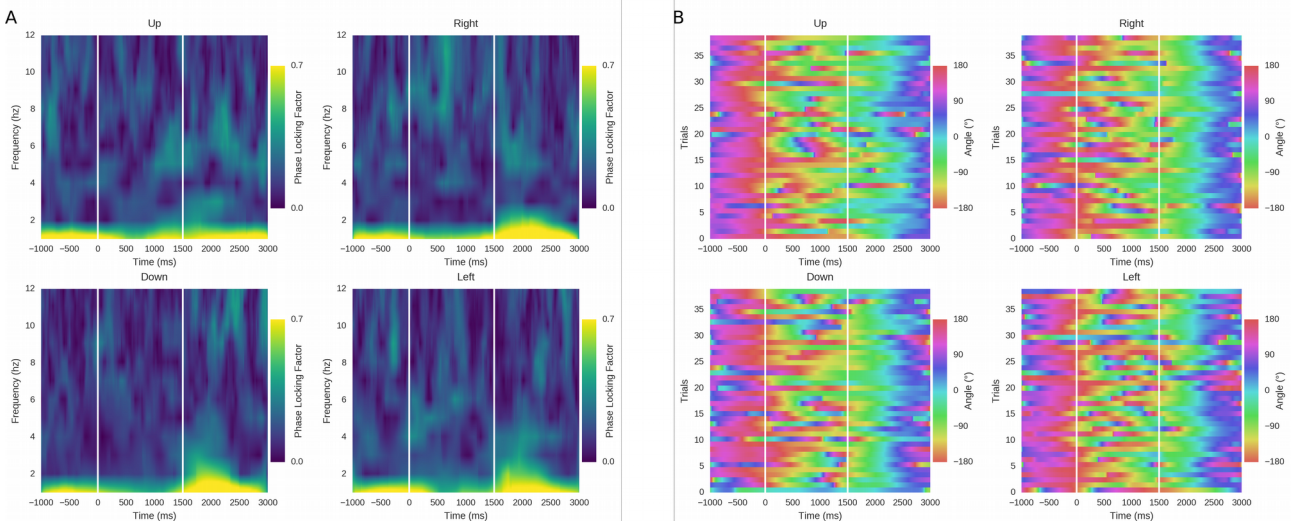


Figure 4. Phase modulations per directions (up/right/down/left) for a premotor seeg site. (A) Phase Locking Factor (PLF) across trials, (B) Single-trial very low frequency phase (VLFC, [0.1, 1.5Hz]) modulation.

4.5.4. Phase-Amplitude Coupling (PAC) features estimation

PAC estimation: First of all, the filter order for extracting phase and amplitude was systematically adapted, using 3 cycles of slow oscillations (for phase) and 6 cycles for amplitude (Bahramisharif et al., 2013). PAC estimations can be estimated by a large variety of measures (Jensen and Colgin, 2007; Canolty and Knight, 2010; Tort et al., 2010; Soto and Jerbi, 2012; Aru et al., 2015). For classification purpose, we tested several of them, mainly the Mean Vector Length (MVL) (Canolty,

2006) and the Kullback-Leiber divergence (KL) (Tort et al., 2010). Both methods provided similar results, but, after slightly adapted the MVL, we obtained PAC estimation and a better decoding accuracies compared to the KL. We generated several artificially coupled signals, with a number of time points equal to our trials length (4001 points per trial) (Tort et al., 2010). On those relatively short signals, the original method for evaluating surrogates , which consist of introducing a random delay on amplitude, was systematically removing real coupling. To solve this limitation, we replaced this method by randomly swapping phase and amplitude trials (Tort et al., 2010). Then, the original modulus is z-scored normalized using the mean and the deviation of 200 generated surrogates.

Time resolution: the phase-amplitude coupling was estimated using the same windows as power features, meaning windows of length of 700ms shifted every 50ms which led to the same number of 67 windows.

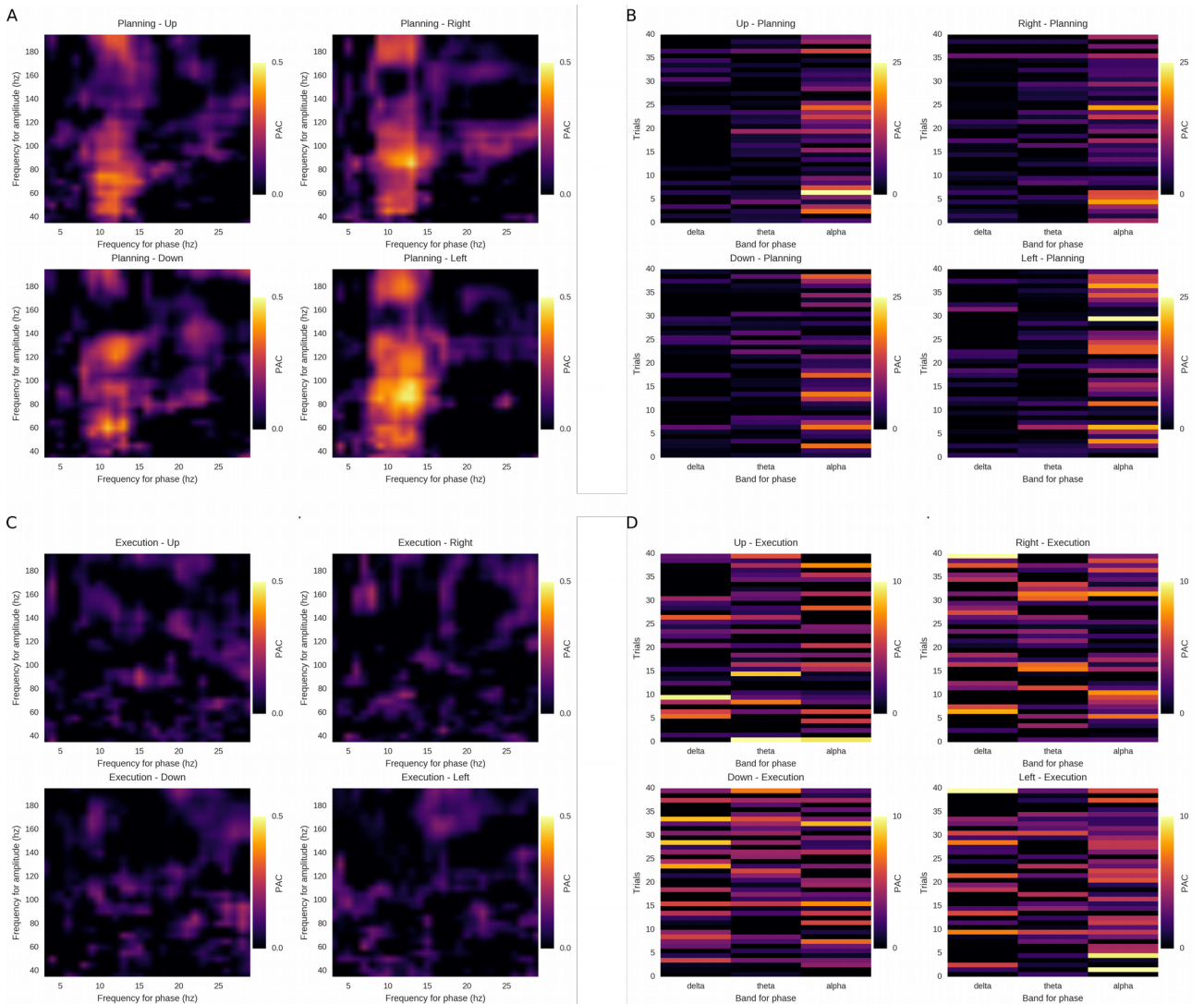


Figure 5. Phase-amplitude coupling (PAC) modulations per directions (up/right/down/left) during planning [0, 1500ms] and execution [1500, 3000ms] phase for a premotor seeg site. (A-C) Comodulogram representing PAC variations as a function of frequency for phase and amplitude during planning (A) and execution (C). (B-D) Single-trial PAC modulations, per direction, for delta [2, 4Hz], theta [5, 7Hz] and alpha [8, 13Hz] phase coupled with high-gamma [60, 200Hz] amplitude for planning (B) and execution phase (D).

4.6. Signal Classification

We explored the feasibility of time resolved decoding directions from human LFP using three strategies from the lowest to the higher dimensionality reduced : *(a)* a single feature approach to evaluate the performance of each feature, *(b)* an intra-site multi-features combination to evaluate the performance of each site, independently of chosen spectral features, *(c)* an inter-sites and inter-features using a feature selection to estimate the final decoding using intracranial recordings. Those three strategies are performed at each of the 67 time points defined above providing an overview of which feature, where and when they are decoding and how reliable they are.

In contrast with EEG and MEG data, inter-subjects cross-validation is not possible for SEEG recordings, because electrodes implantation is specific to each subject. As a consequence, we performed intra-subject cross-validation.

All classifications was performed under Python 3 using scikit-learn package (Pedregosa et al., 2011). Computations were made on the supercomputer Guillimin from the University of Montréal, managed by Calcul Québec and Compute Canada. The operation of this supercomputer is funded by the Canada Foundation for Innovation (CFI), the ministère de l'Économie, de la science et de l'innovation du Québec (MESI) and the Fonds de recherche du Québec - Nature et technologies (FRQ-NT).



4.6.1. Single feature evaluation

Classifier: for all subjects, all bipolar sites, we classified each feature at each of the 67 time window defined above. This procedure cover rest, planning and execution decoding. To this end, we compared the performance of several classification algorithms (Linear Discriminant Analysis (LDA), Naïve Bayes (NB), k-th Nearest Neighbor (KNN), Support Vector Machine (SVM) with linear and Radial Basis Function (RBF) kernels). They all provided similar performances but, because of the high dimensional space features, we finally choose the LDA for it's efficiency and low computer resources. Furthermore, a variety of online BCI (**REF**) studies use the LDA for the reasons above which comfort our choice.

Cross-validation : we compared the decoding influence of Leave-One-Out (LOO) and the 10-folds stratified cross-validation. On our data, LOO provided unstable results while the 10-folds was much more stable. To decrease the deviation of decoding accuracies due to the random choice of training and testing sets, each classification is repeated 10-times which can be summarized as a 10-times 10 stratified k-folds. The stratified argument try to have the same proportion of class labels (in this case, directions) inside each fold which insure that the classifier will be trained on each type of movement. The decoding accuracy is defined as the ratio of the well classified labels under tested labels. The final decoding was obtained by taking the mean of the 10 repetitions and was then expressed in percentage.

Time resolved decoding: a new LDA instance is systematically train and test at each moment. From this procedure we can only conclude if a feature is accurate at one moment of the task time and does not provide informations about time consistency. To address this last point, we performed a temporal generalization.

Temporal Generalization of classification: the temporal generalization is a very elegant method originally proposed by (King and Dehaene, 2014) to evaluate if the the decoding performance of a feature is time specific or if it can be generalized to other time instants. To this end, we trained a classifier at a particular moment in the task (training time axe) and test it at an other time (testing time axe). In this case, training set and testing are well separated. As a consequence, there is no need of cross-validation. Note at this point that the diagonal consist of training and testing at the same

moment, which need a cross validation. For this reason, the diagonal of Figure 8 was systematically not shown for clarity and because the method of the diagonal is different to off-diagonal.

It is not surprising to have similar results inside a window where the task is the same. For example, training during the execution and testing later but still in execution should provide comparable decoding because features shared a consistent information. But training train and test at time where the task differ, tell us if the information contain in the execution and planning is similar. Finally, training on planning and testing during the execution, or the opposite, is different and the temporal generalization tell us if one include the other. Note that the temporal generalization can be performed either on single or multi-features (cf. Figure 8).

4.6.2. Intra-site multi-features

For each seeg bipolar derivation, we combined either power features (6 bands), phase features (4 bands), PAC features (3 bands) or power, phase and PAC (13 bands). Those four combinations are performed using all corresponding number of bands, without any further feature selection. We tried the LDA, the SVM using either the linear or RBF kernels. The last one provided lower results. The LDA and SVM-linear both provided very similar results. Even if the SVM-linear provided a maximum 2% higher compared to the LDA, we chose to show the results of the LDA because it was more consistent with the previous section. We kept the same cross-validation procedure, a 10 times 10 stratified k-folds.

4.6.3. Statistical evaluation and visualization of decoding performances

Statistical evaluation: for each feature, on each seeg site and at each time we computed 1000 permutations thus allowing for statistical assessments with p values as low as 0.001. Each permutation is evaluated by randomly shuffling the label vector (Ojala and Garriga, 2010). The supercomputer was a necessity to compute this large number of permutations, but this method of statistical evaluation lead to more robust p-values compared to a binomial law, because it is data driven (Combrisson and Jerbi, 2015). Using a $p < 0.05$ with 1000 permutations mean that the actual decoding is greater than 95% of permutation decoding accuracies (950). Correction for multiple comparison was assessed by taking the maximum of permutations performances (maximum statistics).

Mapping intracranial EEG decoding to standard MNI brain: each subject's implantation depend on the epileptic focus localization. This particularity of intracranial data make generalization across subjects not as obvious as for EEG or MEG data. In consequence, we developed a Python toolbox, adapted to SEEG recording, to be able to visualize deep intracranial site on a 3-D standard MNI brain (Figure 1A) and to project site's activity on the cortical surface (Figure 1B). Each seeg site is materialized by a color ball into the transparent brain. Cortical projection was obtained by taking the intersection between the cortical surface and a 10 mm radius ball around each site. Some decoding performances are presented as $-\log(p \text{ values})$ (Gunduz et al., 2016). The best is a decoding, the lowest is the p value. The use of the logarithm is a convenient way to rescale and inverse p value intervals. With this transformation, p values between 0.05 and 0.001 are respectively projected into the interval [3, 7]. Finally, every value under 3 (or over 0.05) is systematically turned to gray and is not considered in the projection. 

4.6.4. Multi-features selection

Experimental procedure : The multi-features (MF) consist of finding a group of features that perform better together compared to single feature decoding. At a specific time, the MF procedure tries to find the best possible combination across all feature types (power, phase and phase-amplitude coupling) and across all seeg site per subject. We tried several MF algorithms belonging to the *filter*

or *wrapper* methods (Das, 2001; Guyon and Elisseeff, 2003; Liu et al., 2008). Wrapper methods (like *Select k-best*, *Forward Feature Selection* (FFS) or *Backward Feature Elimination* (BFE)) generally perform better because they are classifier dependent, but they are computationally demanding. Conversely, filter methods (like *FDR*, *PCA*, *minimal-redundancy-maximal-relevance* (Yu and Liu, 2004; Ding and Peng, 2005)) are classifier independent and are much faster which make it a primary choice for large datasets. Considering the number of possible features (>1300 at each time and for each subject), FFS and BFE was not possible to use, especially with permutations. We finally chose to combine a wrapper method (*Select k-best*, with $k \in [1, 10]$) with a filter method (*False Discovery Rate*, FDR with a $p < 0.05$) which are respectively the *SelectKBest()* and the *SelectFdr()* functions of scikit-learn.

Choice of the classifier : we restricted the choice of the classifier either to an LDA or a SVM (with a linear or RBF kernel). We tried to optimize those classifiers (*shrink* parameter of the LDA, the *penalty* parameter *nu* for the linear SVM, and the *nu* and kernel coefficient *gamma* for the SVM with a RBF kernel). SVM provided better results compared to the LDA. Optimized SVM did not provided significantly higher decoding compared to default SVM, and the linear kernel performed better compared to the RBF. As a consequence, we used a non-optimized linear SVM for the whole MF pipeline. As recommended (Hsu et al., 2003), we linearly rescaled each attribute to be zero mean with a unit variance.

Multi-features pipeline : to estimate MF performances, we defined the following pipeline :

1. A first 10-folds cross-validation was defined to generate a training and testing set
2. The training dataset is used to fit parameters of the transformation for data rescaling (*StandardScaler()*), then, this set is rescaled.
3. On the training set, we optimized the MF parameters (number of selected features for the k-best) using a 3-folds cross-validated grid search (*GridSearchCV()*). We then took the union of selected features provided by both methods (*FeatureUnion()*) and got a reduced version of our training set.
4. We trained a classifier on this optimal training set
5. The testing set is rescaled with the same parameters used for the training set. Then, the selected attributes of the training set are used to select those on the testing set.
6. The already trained classifier was finally tested to predict labels on this optimal testing set and turn this prediction into decoding accuracy.
7. **Statistical evaluation of the multi-features pipeline :** this whole pipeline is embedded in a loop of 200 occurrences where, for each occurrence, the label vector is shuffled. Those 200 permutations allows statistical assessments with p values as lows as 0.005.

5. Results

Intro descriptif des figures exemple power / phase / pac

5.1. Decoding motor intentions and execution using power and phase features

Figure 6 shows areas that significantly decode intended or executed limb movements over the four center-out directions using either power or phase features in several frequency bands. In general, lower frequency power features seems to be more accurate for decoding in the planning phase (theta alpha) while higher frequency bands are more execution specific. Interestingly, delta and alpha power features revealed highly significant decoding accuracies essentially during the planning phase in brodmann area (BA) 6 and 9. Supplementary motor area (SMA) also present significant decoding with alpha power during the execution (2100ms). Beta power shows a consistent decoding in parietal lobe (BA 40) during execution (1100, 1600 and 2100ms) which ended with significant decoding in SMA and premotor areas (BA 6) due to the well known beta desynchronization (**REF CHRONE**). High-gamma ([60, 200hz]) shows significant decoding in the SMA, motor (BA4) and premotor (BA6) areas from the end of the planning phase (1100ms) to the end of the execution. Finally, only the VLFC frequency band for phase features present significant areas during the execution in brodmann area 6.

Phase-amplitude coupling features are not presented in this figure even if some SEEG site present significant decoding. Indeed, after visual inspection, PAC did not present a time decoding consistency and significant decoding come the difference between signal deviation.

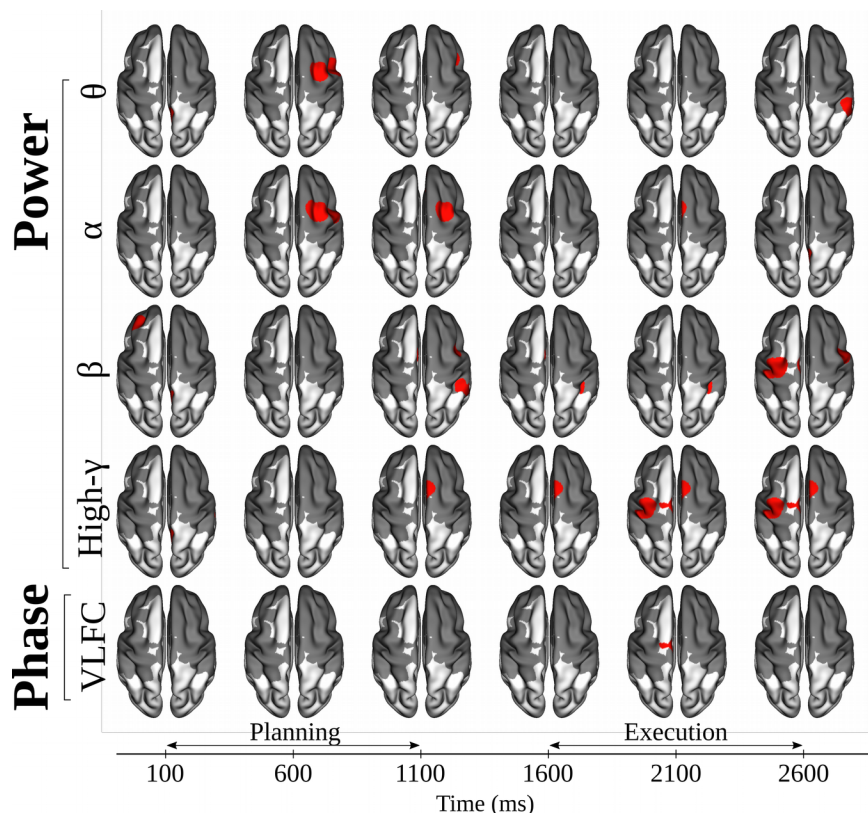


Figure 6. Significant areas presenting 4-directions decoding of intended and executed limb movements using power and phase features over several frequency bands. Power features are presented within delta (δ), theta (θ), alpha (α), beta (β), low-gamma (low- γ) and high-gamma (high- γ) bands and VLFC ([0.1, 1.5Hz]) phase. Each column materialize regularly spaced time instants : three during the planning phase (100ms, 600ms and 1100ms) and three during the execution phase (1600ms, 2100ms and 2600ms). Red areas show significant 4-directions decoding ($p < 0.05$ after correction for multiple comparison using maximum statistics through SEEG sites and time). Non-significant areas are

presented in gray.

5.2. Time resolved power modulations and decoding

The figure 7 shows three examples of time resolved directional tuning (DT) and single feature decoding using power features in alpha and gamma bands. The three intracranial sites (Fig 7D) are respectively located in BA6 (Fig 7A and 7B) and BA9 (Fig 7C). It is important to note that power features are computed on the contralateral hand. The two sites in the right hemisphere (Fig 7A and C) use alpha power and both shared the following pattern : a uniform alpha power across directions during the resting state, a DT during the planning phase and finally, an alpha desynchronization during the execution phase. It should be noted that the alpha power deviation across directions decrease during the execution which means that the desynchronization is consistent across all trials. Moreover, both present significant decodings only during the intention phase. As a matter of fact, the DT for those two sites happened differently. In BA6, the four directions start to be independently modulated from 300ms after Clue 1. The inter-distance is maximized around 1000ms and explains the maximum decoding reach at 44%. in BA9, the non-uniform modulations happened earlier, near Cue 1 and the single feature maximum decoding of 48% is reached around 300ms. In addition, right and left movement intentions are clearly modulated compared to the [-750, -250ms] baseline on the contrary of up and down intentions which seems to be stable.

In comparison, no specific pattern emerge from the resting and planning phase of the gamma power on the BA6 premotor site (Fig 7B). Instead, a non-uniform gamma synchronization across directions happened during the execution only and allowed for a maximum single feature decoding decoding of 63% at 2250ms. Furthermore, the gamma power of vertical directions (up and down) is greater than horizontal directions (right and left). Indeed, gamma power for left limb movement execution is not significantly different from the planning phase. Finally, decoding accuracies start to be greater than corrected permutations from 200ms after the beginning of the execution (Cue 2, 1500ms).

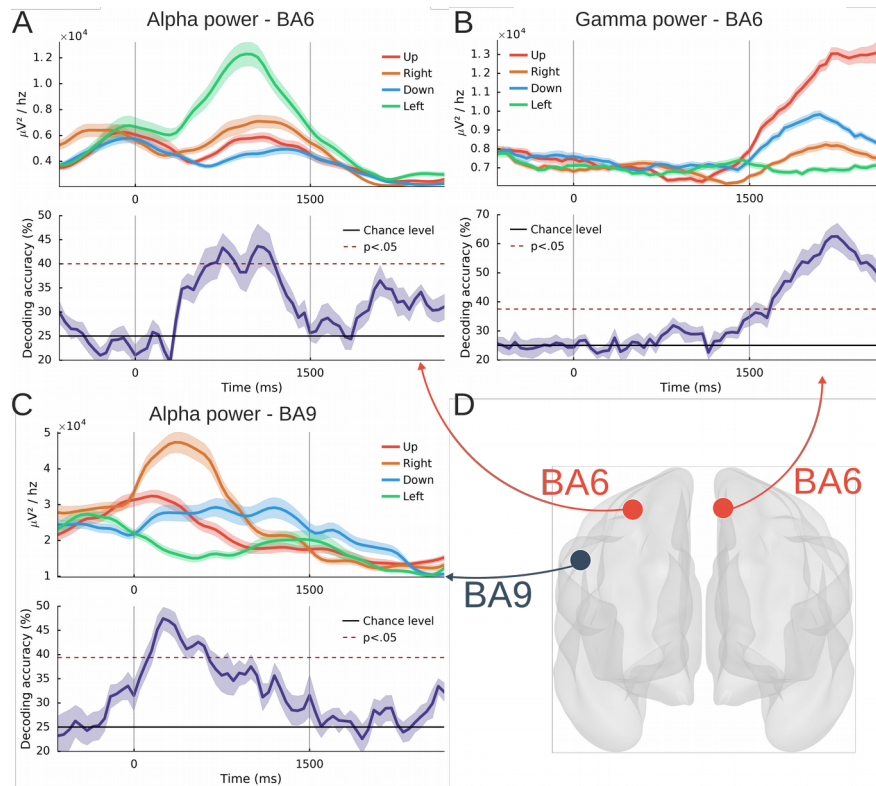


Figure 7. time resolved 4-directions power modulations (up: red; right: brown; down: blue; left: green) and associated decoding accuracies (purple) using a LDA with a 10 times 10 folds cross-validation on three SEEG sites. The power is computed every 50ms using a 700ms windows. The two vertical lines at 0 and 1500ms respectively materialize the beginning of the planning phase (**Cue1**) and the *Go signal* (**Cue 2**). The horizontal black plain line represent the theoretical chance level (4-classes, 25%) and the red dotted line the significance level computed from permutations at $p < 0.05$ after correction for multiple comparison through time points using maximum statistics, (A) alpha power [8,

13hz] on a BA6 site (B) high-gamma [60-200Hz] power on a BA6 site, (C) alpha [8, 13hz] power on a BA9 site, (D) SEEG site locations in a standard MNI brain.

5.3. Temporal Generalization of movement direction decoding

Figure 8 illustrate the use of temporal generalization (TG) using either single or multi power features. Panels A-B-C represent TG using single power features respectively in BA9 (alpha), BA6 (high-gamma) and BA6 (high-gamma) while panel D is the TG for those three combined sites and features. In the first place, the sites used in panels A-B are the same as Fig7 C-B. Additional informations provided by the TG compare to the time-resolved decoding are that both sites are decoding-specific to the intention or execution phase and both don't share directional informations between those motor states. On the contrary, panel C present an other premotor site for which some directional informations are shared. Indeed, a classifier trained during the execution not only provide significant decoding in the execution phase, but in the intention phase too. This site present an non-symmetrical behavior (i.e. a classifier trained during the planning did not lead to a significant decoding during the execution). Finally, the decoding patterns of the three previous TG are conserved when features are combined, with a small decoding improvement and a new emerging significant decoding pattern when the classifier is trained during the intention phase and tested during the execution.

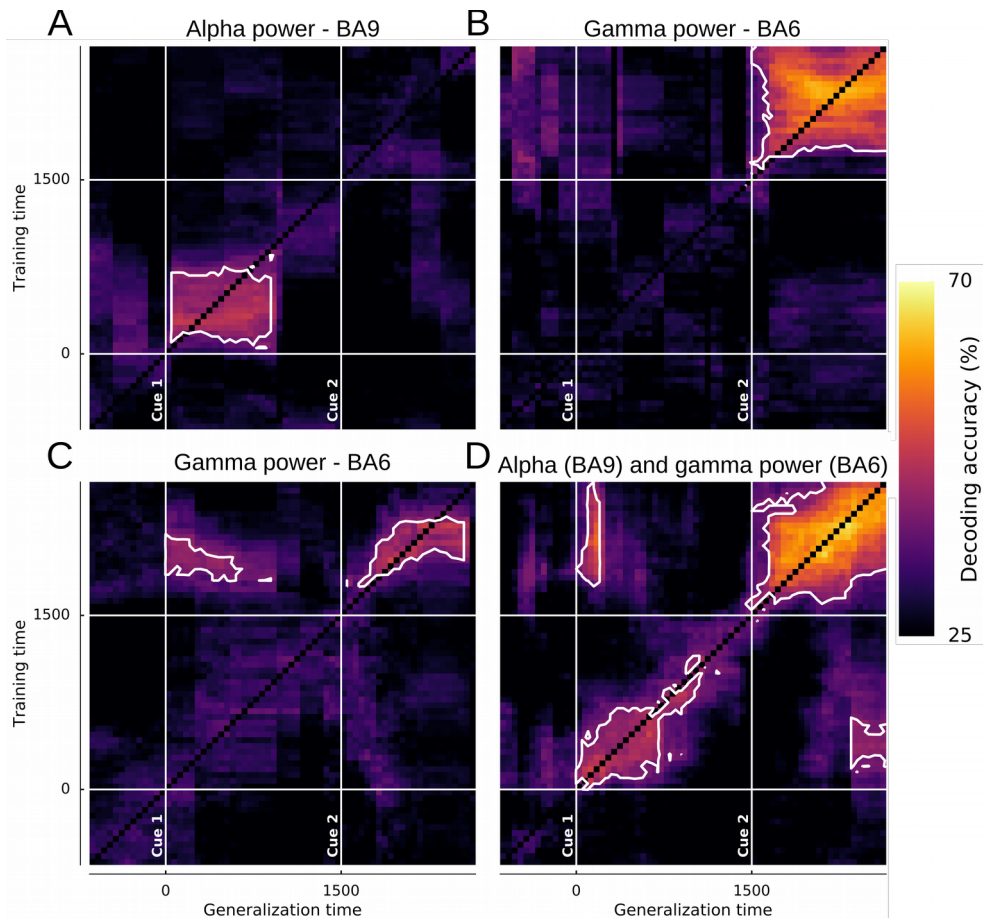


Figure 8. temporal generalization (TG) using power features on three distinct SEEG sites. The vertical and horizontal lines at 0 and 1500ms stand respectively for Cue 1 and Cue 2. White contoured zones delimit significant decodings at $p<0,01$ (binomial test) after bonferroni correction. No decoding are performed on the diagonal, (A) TG of a BA9 site with alpha [8, 13hz] power, (B-C) TG on two distinct premotor (BA6) sites using high-gamma [60, 200hz] power, (D) TG of the three combined sites (alpha BA9 + high-gamma BA6 + high-gamma BA6).

5.4. Feature combination on deep sources

Previous figures illustrate the decoding capabilities using single feature only. Figure 9 shows the

significants decoding performances ($p < 0.05$ after correction for multiple comparison using maximum statistics across SEEG sites and time) by combining, on each intracranial recording site, features coming from several frequency bands without any selection strategy. The first row is obtained by combining the 6 power bands (delta + theta + alpha + beta + low-gamma + high-gamma), the second row represent the decoding using combined phase features in four bands (VLFC + delta + theta + alpha), the third row is obtained by combining the three PAC features coupled with gamma amplitude (delta + theta + alpha) and finally, the last row was obtained by using all possible features (including 6 powers, 4 phase and 3 PAC which lead to 13 features per intracranial site). In the first place, power features revealed a much larger and efficient number of significant features. Premotor, motor and BA40 areas constantly present significant decoding across time but highest decodings non surprisingly happened during execution in BA6 (~60%). In addition, some sites at the BA 6-9-44 junction stop to be significants shortly before the onset of cue 2 (1100ms). As said before, at this significance level, phase and phase-amplitude coupling attributes shows only a small amount of significant area including the primary somatosensory cortex (BA3) during planning using phase combination or frontal areas using PAC (BA10-44). On the other hand, the pattern of the full combination of features is very similar to the power combination. Despite the small contribution of phase and PAC, decoding accuracy reach a maximum of 63% during the execution in BA6.

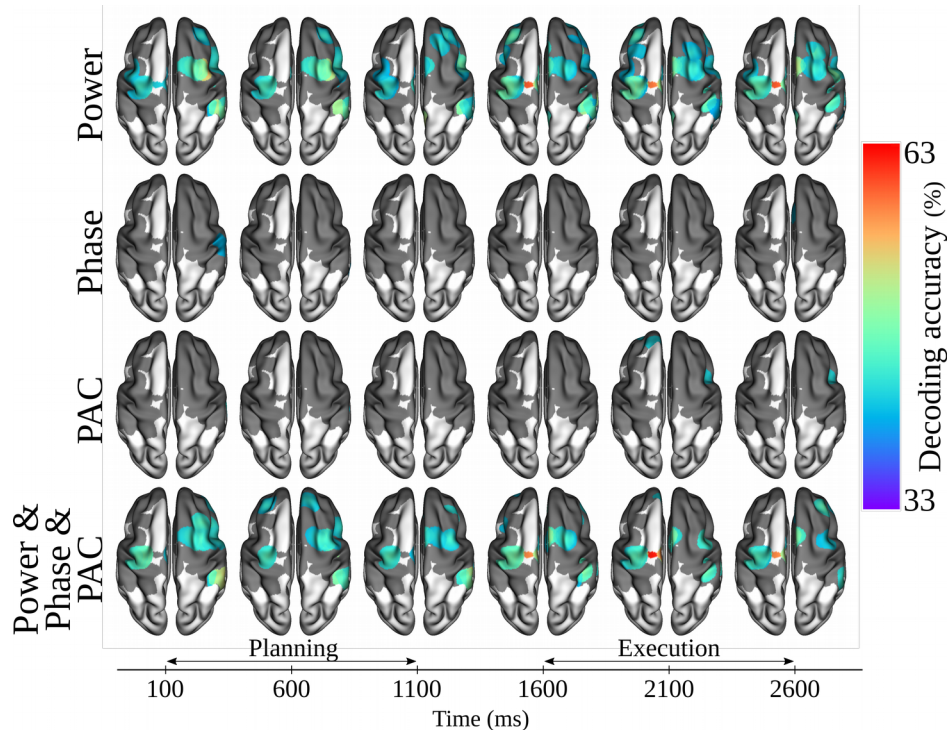


Figure 9. significant decoding accuracies using multi-features per SEEG site for 4 possible combinations at 6 time instants (3 for planning and 3 for execution). For each site, we combined either the 6 power bands (*Power*), either the 4 phase bands (*Phase*), the 3 PAC couple (*PAC*) or all of those features (6 Power + 4 Phase + 3 PAC = 13 features per site).

5.5. Example of a time resolved multi-feature selection

The figure 10 shows an example of the multi-features procedure for subject S1 (right hand motions), obtained by combining feature types (power, phase and PAC across frequency bands) and SEEG sites. It should be noticed that this procedure is launched at each time point leading to a specific and unique set of features. The time resolved decoding accuracy (Fig 10A) present two clear bumps : the first one during the movement intention phase with a maximum reached around 75%, then the DA start decreasing near the Cue 2 onset leading to the second bump in the middle of the execution phase (~82%). Because each time point present a unique set of features, an example of those selected during planning (*t1*) and execution (*t2*) is shown (Fig10 B-C). In the first place, for

both figures, most of the selected features are power with only a few of them being either phase or PAC. During planning, selected features are uniformly distributed across both hemispheres with a majority of low frequency power (beta, alpha and theta) in BA9 and BA6. Interestingly, the VLFC phase in BA6 and the delta/gamma coupling in BA9 seems to be the more relevant non-power features. In contrast, motor execution present less frontal features (BA9) but most of those selected are concentrated in the contralateral premotor area (BA6). Unlike planning, execution seems to be more decoded using high-frequency power features (high and low-gamma) and delta/gamma coupling in the BA8.

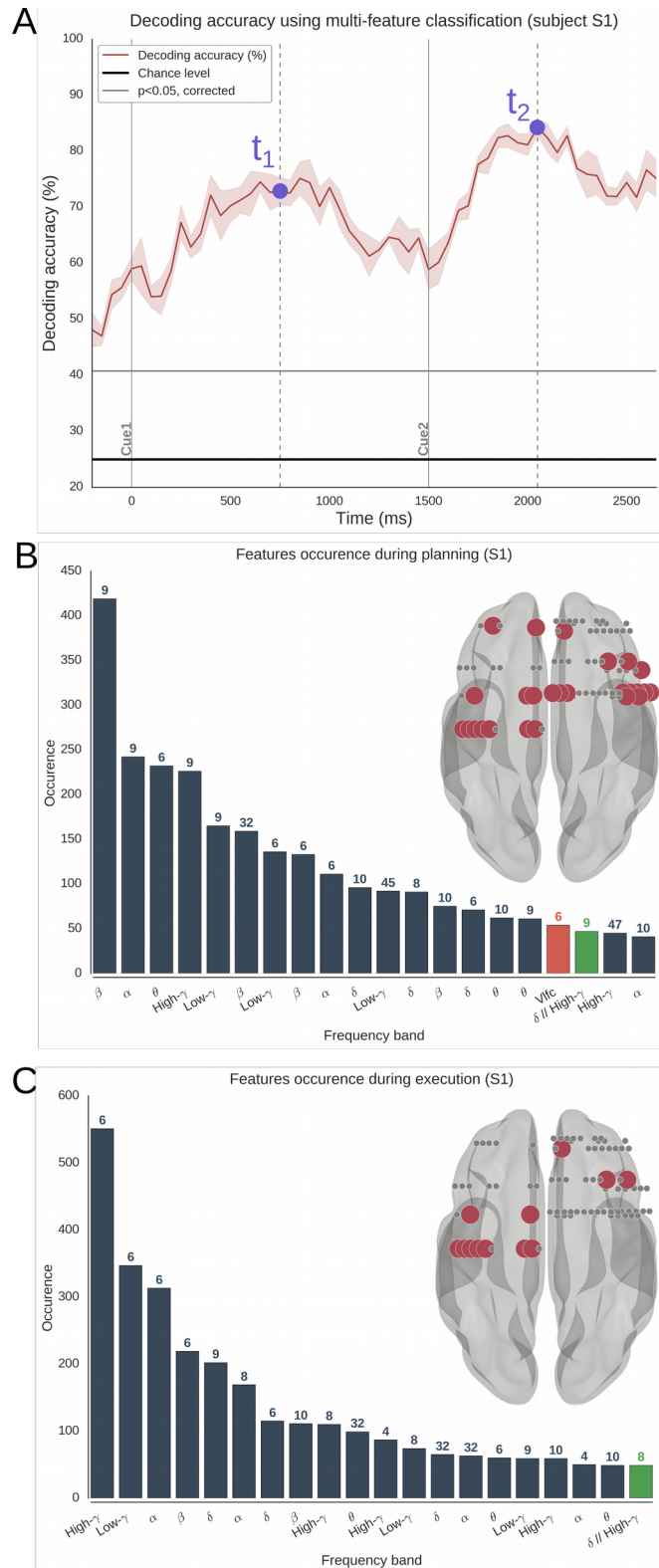


Figure 10. Combining all possible features and seeg sites of subject S1 using the multi-features procedure, (A) Time resolved decoding accuracy and associated deviation using the MF selection. Cue 1 and Cue 2 are materialized with two

solid gray lines. t_1 (750ms) and t_2 (2048ms) are respectively two chosen time instants during planning and execution. The horizontal solid gray line is the corrected decoding accuracy ($p < 0,05$ corrected using maximum statistics across time points) obtained by randomly shuffling the label vector (permutations), (B-C) 20 most selected features respectively at t_1 (planning) and t_2 (execution). For each barplot, the y-axis show the number of times a feature was selected (*occurrence*) and the x-axis show the name of the frequency band. Blue bar stand for Power, red for Phase and green for Phase-amplitude coupling features. On top of each bar, there is the associated brodmann area where the site come from. Finally, the transparent brain summarize sites location. Red dots represents all different selected site (without carrying the feature type information) and gray dots represent non-selected sites.

5.6. Decoding results of the multi-feature procedure across subjects

The figure 11 shows a final overview of the best decoding accuracies (Fig 11A) and most recurrent selected features (Fig 11B) across subjects, get by combining features and intracranial recording sites. Both decoding intentions and motor executions reached a maximum of 86% (S1). In general, the DA of execution is non-surprisingly higher or equal than planning with the exception of subject 5. This subject present a 14% difference between both DA (84% for planning and 70% for execution) which is to say that this subject has a more intention specific SEEG implantation. Subjects 4 and 6 did not present a significant maximum decoding even with the multi-features procedure. For decoding the execution, high frequency power (i.e. low and high gamma) were the most selected feature especially in pre and primary motor area BA4-6-8-11. By comparison, decoding the four directions during the intention phase were largely achieved using lower power frequency (i.e. delta, theta, alpha and beta) in premotor, frontal and parietal area (BA6-9-40).

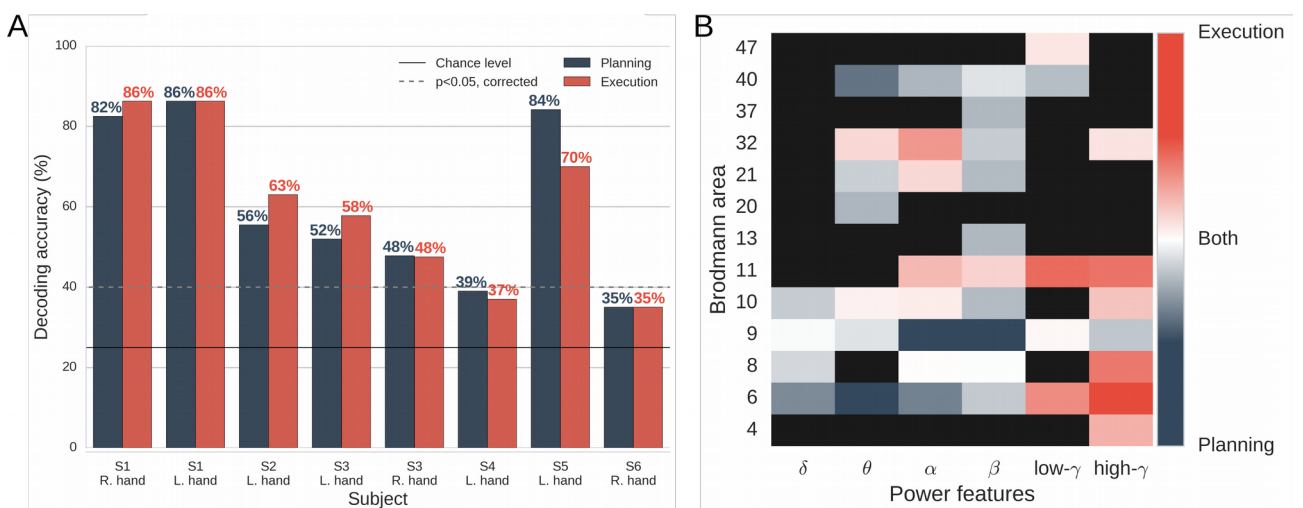


Figure 11. Best decoding accuracies for planning (blue) and execution (red) across subjects using the multi-features selection, **(A)** Best decoding accuracies per subject for intention and execution. The solid black line materialize the theoretical chance level of a 4-class classification problem (25%) and the dotted gray line (~40%), the statistical chance level at $p<0.05$ (corrected using maximum statistics across subjects), **(B)** Most recurrent selected power features during the multi-features procedure as a function of brodmann area. Power features that are specific to the execution, planning or both are respectively turned into red, blue and white. Black rectangles stand for no selected features.

6. Discussion

The present study was intended to decode from rare intracranial recordings the planning and the execution of four directions center-out movements. For both periods, we implemented both well-established (i.e. power features) and emerging decoding approaches (i.e. phase and phase-amplitude coupling). The data showed that the four directions center-out movements were inferred with a maximum rate of 86% for the execution phase but, over and above, during the movement preparation with the same decoding rate success of 86%. Interestingly, we showed that some intracranial sites were specifically relevant to decode the movement direction during the motor preparation, while some were more relevant to decode the movement direction during the execution. Eventually, some sites decoded the movement direction with a high accuracy for both preparation and execution. From a decoding perspective, the highest decoding accuracies were obtained by combining a series of signal features (e.g., power, phase and phase-amplitude coupling) throughout a series of brain sites (e.g. motor, premotor but also non-motor areas).

6.1. Unraveling the role of power, phase and phase-amplitude coupling

It is well established that power signals carried directional informations that can be then used for decoding or in a BCI context (Rickert, 2005; Waldert et al., 2008). In addition, phase signals can be used to infer hand position, velocity and acceleration through low frequency phase (Jerbi et al., 2007; Hammer et al., 2013). For all that, there is no studies to our knowledge that explored such a variety of features and, especially extracting and used PAC as a potentially directions decoding feature. The present study reveals that the majority of the decoding features was in fact power (Fig 6). In addition, we showed that the very low frequency phase was the only non-power feature which allowed directions classification (Fig 6) but only during the execution phase. It has been shown that phase-amplitude coupling does not represent the movement type (Yanagisawa et al., 2012). We found some significant decoding PAC but after a visual inspection, none of them showed a consistent decoding across the time axis and a clear difference in direction modulation (as Fig 6). We previously showed that PAC can be used to decode motor state (Combrisson et al., 2017) but the present study seems to reveal that PAC do not carry directional informations or at least, not with the accuracy of power or VLFC phase features.

6.2. Involvement of non-primary motor areas

As said before, the classification using single power features showed significant decoding in both execution and planning phase. Indeed, high-gamma power in primary and premotor cortex seems to be the best choice in order to differentiate the four directions during the execution phase (Fig 6-7-11B). Because of its intracranial implantation, one subject showed a 70% decoding during the execution using only the high-gamma power in Brodmann area 6. In addition, the alpha power in the inferior parietal lobule reached a 50% decoding rate while the subject was planning one over the four possible directions (Fig 6). We found that planned directions were much better decoded using lower power frequencies (first using the alpha and beta bands then, in a lesser extent, using delta and theta bands). An important point, prominent areas for decoding the four directions during the planning phase was the Brodmann area 9, 40 and 6. BA 9 is known to be involved in motor behavior such as planning directions (Gunduz et al., 2016). BA 40, part of the posterior parietal cortex, is also involved in motor planning (Snyder et al., 1997; Andersen and Buneo, 2002; Buneo and Andersen, 2006; Andersen and Cui, 2009) and in the transformation of sensory informations into motor commands especially for long-term coding of spatial relationships (Karnath, 2001; Buneo and Andersen, 2006).

6.3. Features specificity and complementarity

We went one step further by asking the question of decoding specificity (i.e. the ability to decode only during planning, execution or in both phase) and the complementarity (i.e. features association that perform better compare to single feature). To illustrate this question, we used the temporal generalization (King and Dehaene, 2014) and shows that some sites perform exclusively during certain phase (i.e. Fig 8A-B), in both phases (Fig 8C) and that their association allows a continuous 4-directions dissociation (Fig 8D). For a larger scale investigation, we tried several multi-features strategies. First, we combined features per SEEG site (Fig 9). Without any selection algorithm, we combined either power only, phase only, PAC only or the three grouped. This type of combination did not lead to a significant decoding improvement. The decoding increase come from the site diversity. Indeed, we took the union derived from the k-best and FDR feature selection in order to combine features across intracranial recordings. By applying this procedure at each time point, we showed an example of time resolved decoding leading to a maximum of 82% during the execution and, more importantly, 75% during the intention phase (Fig 10). Multi-features analysis across subjects highlighted how much the decoding depends on the intracranial implantation (Fig 11A). While some subjects have seen their decoding reach 86%, others did not present any significant results even with this feature selection. Finally, we grouped the most selected features across subjects according to their decoding specificity (Fig 11B). High-frequency power, especially in motor and premotor area seems to be much more specific to the execution while lower power bands in BA6-9-40 appears to be specific to the intentions decoding.

6.4. Limitations and future paths

The results of this study have a number of limitations. Intracranial recordings provide high quality signals at the cost of a heterogeneous and incomplete coverage of brain areas across patients. Even with more than 500 recordings sites, areas are not equally represented. The coverage over the six subjects (see Fig1) offer a correct cover of frontal (with the right hemisphere over represented compare to the left hemisphere) and central areas but parietal cortex is under represented. Moreover, four over the six patients had uni-lateral implantations and the two others had a non-symmetrical one. Because of this typical invasive recording limitation, it was not possible to separate contra and ipsilateral effect on directions decoding and it would be a great benefit to see if ipsilateral movement also represent hand actions (Gallivan et al., 2013). This should be addressed using EEG or MEG recordings using the same center-out paradigm. Those patients suffered from a drug-resistant epilepsy which might limit the generalizability to healthy subjects. This critical point was assessed after a visual inspection and by systematically removing electrodes that present typical epileptic waveforms (i.e. epileptic spikes).

In our center-out paradigm, subjects were asked to plan an imposed direction (i.e. prepare the hand movement they will have to execute later). Therefore, the task design did not allow to distinguish between motor plans and visual stimulus encoding as both were congruent.

- Heterogeneous and incomplete coverage of brain areas across the patients + epilepsie d'origine résistante.
- The task design did not allow us to distinguish between motor plans and visual stimulus encoding as both were congruent. Previous studies have explored this (Refs+discuss).
- Décodage MF intra sujet et pas de pool de sujets comme en EEG ou MEG à cause de l'implantation
- Alignement sur le go signal?

Acknowledgments

Etienne Combrisson was supported in part by a PhD Scholarship awarded by the Ecole Doctorale Inter-Disciplinaire Sciences-Santé (EDISS), Lyon, France, and by PhD funding from the Natural Sciences and Engineering Research Council of Canada (NSERC). This work was partly performed within the framework of the LABEX CORTEX (ANR-11-LABX-0042) of Université de Lyon, within the program ANR-11-IDEX-0007, and by the ANR (project FORCE, ANR-13-TECS-0013-01), SEMAINE, the Human Brain Project (Human intracerebral database, grant number 604102) to J.-P. Lachaux; We acknowledge support from the Brazilian Ministry of Education (CAPES grant 1719-04-1), the Foundation pour la Recherche Médicale (FRM, France) and the Fulbright Commission to J.L.P. Soto, and funding from the Canada Research Chairs program and a Discovery Grant (RGPIN-2015-04854) awarded by the Natural Sciences and Engineering Research Council of Canada to K.J. The authors are grateful for the collaboration of the patients and clinical staff at the Epilepsy Department of the Grenoble University Hospital.

Conflict of interest

The authors declare that there is no conflict of interests regarding the publication of this paper.

7. References

- Andersen RA, Buneo CA (2002) Intentional maps in posterior parietal cortex. *Annu Rev Neurosci* 25:189–220.
- Andersen RA, Cui H (2009) Intention, Action Planning, and Decision Making in Parietal-Frontal Circuits. *Neuron* 63:568–583.
- Aru J, Aru J, Priesemann V, Wibral M, Lana L, Pipa G, Singer W, Vicente R (2015) Untangling cross-frequency coupling in neuroscience. *Curr Opin Neurobiol* 31:51–61.
- Babiloni C, Babiloni F, Carducci F, Cincotti F, Rosciarelli F, Arendt-Nielsen L, Chen ACN, Rossini PM (2002) Human brain oscillatory activity phase-locked to painful electrical stimulations: A multi-channel EEG study. *Hum Brain Mapp* 15:112–123.
- Bahramisharif A, van Gerven MAJ, Aarnoutse EJ, Mercier MR, Schwartz TH, Foxe JJ, Ramsey NF, Jensen O (2013) Propagating Neocortical Gamma Bursts Are Coordinated by Traveling Alpha Waves. *J Neurosci* 33:18849–18854.
- Ball T, Schulze-Bonhage A, Aertsen A, Mehring C (2009) Differential representation of arm movement direction in relation to cortical anatomy and function. *J Neural Eng* 6:16006.
- Bastin J, Deman P, David O, Gueguen M, Benis D, Minotti L, Hoffman D, Combrisson E, Kujala J, Perrone-Bertolotti M, Kahane P, Lachaux J-P, Jerbi K (2016) Direct Recordings from Human Anterior Insula Reveal its Leading Role within the Error-Monitoring Network. *Cereb Cortex:bjh352*.
- Berens P, others (2009) CircStat a MATLAB toolbox for circular statistics. *J Stat Softw* 31:1–21.
- Buneo CA, Andersen RA (2006) The posterior parietal cortex: sensorimotor interface for the planning and online control of visually guided movements. *Neuropsychologia* 44:2594–2606.
- Canolty RT (2006) High Gamma Power Is Phase-Locked to Theta. *science* 1128115:313.
- Canolty RT, Knight RT (2010) The functional role of cross-frequency coupling. Available at: https://www.researchgate.net/profile/Ryan_Canolty/publication/47382016_The_functional_role_of_cross-frequency_coupling/links/548651f00cf2ef34478bf713.pdf [Accessed March 18, 2016].
- Chao (2010) Long-term asynchronous decoding of arm motion using electrocorticographic signals in monkey. *Front Neuroengineering* Available at: <http://journal.frontiersin.org/article/10.3389/fneng.2010.00003/abstract> [Accessed April 13, 2017].
- Combrisson E, Jerbi K (2015) Exceeding chance level by chance: The caveat of theoretical chance levels in brain signal classification and statistical assessment of decoding accuracy. *J Neurosci Methods* 250:126–136.
- Combrisson E, Perrone-Bertolotti M, Soto JL, Alamian G, Kahane P, Lachaux J-P, Guillot A, Jerbi K (2017) From intentions to actions: Neural oscillations encode motor processes through phase, amplitude and phase-amplitude coupling. *NeuroImage* 147:473–487.

- Das S (2001) Filters, wrappers and a boosting-based hybrid for feature selection. In: ICML, pp 74–81. Citeseer. Available at: <http://citeseerx.ist.psu.edu/viewdoc/download?doi=10.1.1.124.5264&rep=rep1&type=pdf> [Accessed July 6, 2016].
- Delorme A, Makeig S (2004) EEGLAB: an open source toolbox for analysis of single-trial EEG dynamics including independent component analysis. *J Neurosci Methods* 134:9–21.
- Ding C, Peng H (2005) Minimum Redundancy Feature Selection from Microarray Gene Expression Data. Available at: http://crd-legacy.lbl.gov/~hpeng/papersall/2003_feasel_2003-8-1_chris.pdf [Accessed December 16, 2013].
- Gallivan JP, McLean DA, Flanagan JR, Culham JC (2013) Where one hand meets the other: limb-specific and action-dependent movement plans decoded from preparatory signals in single human frontoparietal brain areas. *J Neurosci* 33:1991–2008.
- Gallivan JP, McLean DA, Valyear KF, Pettypiece CE, Culham JC (2011) Decoding Action Intentions from Preparatory Brain Activity in Human Parieto-Frontal Networks. *J Neurosci* 31:9599–9610.
- Georgopoulos A, Schwartz A, Kettner R (1986) Neuronal population coding of movement direction. *Science* 233:1416–1419.
- Georgopoulos AP, Kalaska JF, Caminiti R, Massey JT (1982) On the relations between the direction of two-dimensional arm movements and cell discharge in primate motor cortex. *J Neurosci* 2:1527–1537.
- Gunduz A, Brunner P, Sharma M, Leuthardt EC, Ritaccio AL, Pesaran B, Schalk G (2016) Differential roles of high gamma and local motor potentials for movement preparation and execution. *Brain-Comput Interfaces* 3:88–102.
- Guyon I, Elisseeff A (2003) An introduction to variable and feature selection. *J Mach Learn Res* 3:1157–1182.
- Hamamé CM, Vidal JR, Perrone-Bertolotti M, Ossandón T, Jerbi K, Kahane P, Bertrand O, Lachaux J-P (2014) Functional selectivity in the human occipitotemporal cortex during natural vision: Evidence from combined intracranial EEG and eye-tracking. *NeuroImage* 95:276–286.
- Hammer J, Fischer J, Ruescher J, Schulze-Bonhage A, Aertsen A, Ball T (2013) The role of ECoG magnitude and phase in decoding position, velocity, and acceleration during continuous motor behavior. *Front Neurosci* 7 Available at: <http://www.frontiersin.org/Journal/10.3389/fnins.2013.00200/full> [Accessed January 27, 2014].
- Heldman DA, Wang W, Chan SS, Moran DW (2006) Local Field Potential Spectral Tuning in Motor Cortex During Reaching. *IEEE Trans Neural Syst Rehabil Eng* 14:180–183.
- Hsu C-W, Chang C-C, Lin C-J, others (2003) A practical guide to support vector classification.
- Jensen O, Colgin LL (2007) Cross-frequency coupling between neuronal oscillations. *Trends Cogn Sci* 11:267–269.
- Jerbi K, Lachaux J-P, Karim N, Pantazis D, Leahy RM, Garnero L, Baillet S, others (2007) Coherent neural representation of hand speed in humans revealed by MEG imaging. *Proc Natl Acad Sci* 104:7676–7681.

Jerbi K, Ossandón T, Hamamé CM, Senova S, Dalal SS, Jung J, Minotti L, Bertrand O, Berthoz A, Kahane P, Lachaux J-P (2009) Task-related gamma-band dynamics from an intracerebral perspective: Review and implications for surface EEG and MEG. *Hum Brain Mapp* 30:1758–1771.

Jerbi K, Vidal JR, Ossandon T, Dalal SS, Jung J, Hoffmann D, Minotti L, Bertrand O, Kahane P, Lachaux J-P (2010) Exploring the electrophysiological correlates of the default-mode network with intracerebral EEG. *Front Syst Neurosci* 4:27.

Kahane P, Landré E, Minotti L, Francione S, Ryvlin P (2006) The Bancaud and Talairach view on the epileptogenic zone: a working hypothesis. *Epileptic Disord Int Epilepsy J Videotape* 8:S16–26.

Kahane P, Minotti L, Hoffmann D, Lachaux J-P, Ryvlin P (2003) Invasive EEG in the definition of the seizure onset zone: depth electrodes. *Handb Clin Neurophysiol* 3:109–133.

Karnath H-O (2001) New insights into the functions of the superior temporal cortex. *Nat Rev Neurosci* 2:569.

King J-R, Dehaene S (2014) Characterizing the dynamics of mental representations: the temporal generalization method. *Trends Cogn Sci* 18:203–210.

Lachaux JP, Rudrauf D, Kahane P (2003) Intracranial EEG and human brain mapping. *J Physiol-Paris* 97:613–628.

Lakatos P (2005) An Oscillatory Hierarchy Controlling Neuronal Excitability and Stimulus Processing in the Auditory Cortex. *J Neurophysiol* 94:1904–1911.

Leuthardt EC, Schalk G, Wolpaw JR, Ojemann JG, Moran DW (2004) A brain–computer interface using electrocorticographic signals in humans. *J Neural Eng* 1:63.

Liu J, Newsome WT (2006) Local Field Potential in Cortical Area MT: Stimulus Tuning and Behavioral Correlations. *J Neurosci* 26:7779–7790.

Liu J, Ranka S, Kahveci T (2008) Classification and feature selection algorithms for multi-class CGH data. *Bioinformatics* 24:i86–i95.

Mehring C, Rickert J, Vaadia E, de Oliveira SC, Aertsen A, Rotter S (2003) Inference of hand movements from local field potentials in monkey motor cortex. *Nat Neurosci* 6:1253–1254.

Ojala M, Garriga GC (2010) Permutation tests for studying classifier performance. *J Mach Learn Res* 11:1833–1863.

Ossandon T, Jerbi K, Vidal JR, Bayle DJ, Henaff M-A, Jung J, Minotti L, Bertrand O, Kahane P, Lachaux J-P (2011) Transient Suppression of Broadband Gamma Power in the Default-Mode Network Is Correlated with Task Complexity and Subject Performance. *J Neurosci* 31:14521–14530.

Pedregosa F, Varoquaux G, Gramfort A, Michel V, Thirion B, Grisel O, Blondel M, Prettenhofer P, Weiss R, Dubourg V, Vanderplas J, Passos A, Cournapeau D, Brucher M, Perrot M, Duchesnay E (2011) Scikit-learn: Machine Learning in Python. *J Mach Learn Res* 12:2825–2830.

Perrone-Bertolotti M, Kujala J, Vidal JR, Hamame CM, Ossandon T, Bertrand O, Minotti L,

- Kahane P, Jerbi K, Lachaux J-P (2012) How silent is silent reading? Intracerebral evidence for top-down activation of temporal voice areas during reading. *J Neurosci* 32:17554–17562.
- Rickert J (2005) Encoding of Movement Direction in Different Frequency Ranges of Motor Cortical Local Field Potentials. *J Neurosci* 25:8815–8824.
- Schalk G, Kubanek J, Miller K, Anderson N, Leuthardt E, Ojemann J, Limbrick D, Moran D, Gerhardt L, Wolpaw J (2007) Decoding two-dimensional movement trajectories using electrocorticographic signals in humans. *J Neural Eng* 4:264.
- Snyder LH, Batista AP, Andersen RA (1997) Coding of intention in the posterior parietal cortex. *Nature* 386:167–170.
- Soto JL, Jerbi K (2012) Investigation of cross-frequency phase-amplitude coupling in visuomotor networks using magnetoencephalography. In: Engineering in Medicine and Biology Society (EMBC), 2012 Annual International Conference of the IEEE, pp 1550–1553. IEEE. Available at: http://ieeexplore.ieee.org/xpls/abs_all.jsp?arnumber=6346238 [Accessed March 18, 2016].
- Talairach J, Tournoux P (1993) Referentially oriented cerebral MRI anatomy: an atlas of stereotaxic anatomical correlations for gray and white matter. Thieme.
- Tallon-Baudry C, Bertrand O, Delpuech C, Pernier J (1996) Stimulus specificity of phase-locked and non-phase-locked 40 Hz visual responses in human. *J Neurosci* 16:4240–4249.
- Tankus A, Yeshurun Y, Flash T, Fried I (2009) Encoding of speed and direction of movement in the human supplementary motor area. *J Neurosurg* 110:1304–1316.
- Taylor DM (2002) Direct Cortical Control of 3D Neuroprosthetic Devices. *Science* 296:1829–1832.
- Tort ABL, Komorowski R, Eichenbaum H, Kopell N (2010) Measuring Phase-Amplitude Coupling Between Neuronal Oscillations of Different Frequencies. *J Neurophysiol* 104:1195–1210.
- Vidal JR, Freyermuth S, Jerbi K, Hamamé CM, Ossandon T, Bertrand O, Minotti L, Kahane P, Berthoz A, Lachaux J-P (2012) Long-distance amplitude correlations in the high gamma band reveal segregation and integration within the reading network. *J Neurosci* 32:6421–6434.
- Vidal JR, Perrone-Bertolotti M, Levy J, De Palma L, Minotti L, Kahane P, Bertrand O, Lutz A, Jerbi K, Lachaux J-P (2014) Neural repetition suppression in ventral occipito-temporal cortex occurs during conscious and unconscious processing of frequent stimuli. *Neuroimage* 95:129–135.
- Waldert S, Braun C, Preissl H, Birbaumer N, Aertsen A, Mehring C (2007) Decoding performance for hand movements: EEG vs. MEG. In: Engineering in Medicine and Biology Society, 2007. EMBS 2007. 29th Annual International Conference of the IEEE, pp 5346–5348. IEEE. Available at: http://ieeexplore.ieee.org/xpls/abs_all.jsp?arnumber=4353549 [Accessed July 4, 2014].
- Waldert S, Preissl H, Demandt E, Braun C, Birbaumer N, Aertsen A, Mehring C (2008) Hand Movement Direction Decoded from MEG and EEG. *J Neurosci* 28:1000–1008.
- Yanagisawa T, Yamashita O, Hirata M, Kishima H, Saitoh Y, Goto T, Yoshimine T, Kamitani Y

(2012) Regulation of Motor Representation by Phase–Amplitude Coupling in the Sensorimotor Cortex. *J Neurosci* 32:15467–15475.

Yu L, Liu H (2004) Redundancy based feature selection for microarray data. In: Proceedings of the tenth ACM SIGKDD international conference on Knowledge discovery and data mining, pp 737–742. ACM. Available at: <http://dl.acm.org/citation.cfm?id=1014149> [Accessed July 5, 2016].